-- Electronic Supplementary Information --

Role of Liquid Water Distribution in MgO Hydroxylation

Vitalii Starchenko[1*], Sai_Adapa[1], Lawrence. M. Anovitz[1], Ilia Ivanov[2], Andrew G. Stack[1], Ke Yuan[1], Juliane Weber[1]

[1] Chemical Science Division, Oak Ridge National Laboratory, Oak Ridge, USA

[2] Center for Nanophase Materials Sciences, Oak Ridge National Laboratory, Oak Ridge, USA

[*]Corr. auth.: starchenkov@ornl.gov

1. Computational details

We adopt a phase-field modeling approach in which the liquid-vapor system is modeled as a van der Waals fluid. In this model the vapor-liquid density, ρ, is an order parameter. The generalized Helmholtz free energy consists of thermodynamic specific free energy, $f_{th}(\rho)$, and nonlocal specific free energy, $f_{nl}(\nabla\rho)$, therefore we define the free-energy functional in terms of ρ and $\nabla\rho$

$$F(\rho,\nabla\rho) = \int_V [f_{th}(\rho) + f_{nl}(\nabla\rho)]dV \#(S1)$$

According to the van der Waals thermodynamic theory of capillarity[1] the homogeneous part of the free energy functional can be expressed as

$$f_{th} = \frac{\rho RT}{M_w}\ln\frac{c_1\rho}{1-c_1\rho} - c_2\rho, \#(S2)$$

where R – is the gas constant, T is temperature, M_w – molar volume of water, $c_1 = \frac{b}{M_w}$ and $c_2 = \frac{a}{RT_cM_w}$ are the van der Waals equation of state parameters, which include excluded volume constant, b, and molecular interaction constant, a, and T_c is a critical temperature for water.

Nonlocal part of the specific free energy is

$$f_{nl}(\nabla\rho) = \frac{1}{2}T\varepsilon(\nabla\rho)^2, \#(S3)$$

where $\varepsilon = \frac{RT\delta^2}{M_w}v$ is related to the thickness of the smooth interface, in which, v is the specific volume of the liquid phase, and δ is a typical interface thickness. The parameter δ can be estimated using van der

Waals formulation[1] for the surface tension, γ, at the liquid-vapor interface at local equilibrium in similar way it is reported by Lamorgese and Mauri[2]

$$\gamma = \int T\varepsilon(\nabla\rho)^2 dl = \frac{RT\delta}{M_w} v(\rho_l - \rho_v)_{eq}^2$$

where $(\rho_l - \rho_v)_{eq}$ is the difference in liquid and vapor densities at equilibrium. Since temperature is a part of the equation, the interface thickness will be different in simulations at different temperatures (Table S1).

In this work we assume the conditions to be isothermal, therefore the governing equations for the system include mass conservation and momentum conservation

$$\partial_t \rho + \nabla \cdot (\rho u) = 0 \#(S4)$$

$$\partial_t(\rho u) + \nabla \cdot (\rho u \otimes u) = \nabla \cdot \left(\eta\left[\nabla u + \nabla u^T\right]\right) - \rho\nabla\mu^{NC} + \rho g \#(S5)$$

where u is the fluid velocity, η is the dynamic viscosity, g is the gravitational acceleration, and μ^{NC} is the nonclassical chemical potential.[3] The nonclassical chemical potential is defined as a variational derivative of the free energy functional (**equation S1**)

$$\mu^{NC} = \frac{\delta F}{\delta \rho} = \partial_\rho f_{th} - \nabla \cdot (T\varepsilon\nabla\rho)$$

Chemical potential can be expressed as $\mu = \partial_\rho f_{th}$, and, since we consider isothermal conditions, the equation of state, which defines the pressure, P, closes the conservation equations

$$P = \rho\mu - f_{th} \#(S6)$$

To simplify calculations, we fit the **equation S2** with the function which reproduces the shape of the double well potential

$$f_{th}^{fit} = C_1(\rho - C_2)^2(\rho - C_3)^2 - C_4\rho \#(S7)$$

where C_1, C_2, C_3, and C_4 are constants.

The effect of the substrate is modelled as a boundary condition for the density field. The Young-Laplace equation in combination with expression for the surface tension provides the boundary condition for density, ρ_b, which defines the contact angle between substrate, vapor, and liquid:

$$\gamma = \int_{-\infty}^{\infty} T\varepsilon\left(\frac{\partial\rho}{\partial z}\right)^2 dz = \int_{\rho_V}^{\rho_L} \sqrt{2T\varepsilon f_{th}(\rho)}\, d\rho \#(S8)$$

where ρ_L is the density of liquid and ρ_V is the density of vapor. The implementation of the boundary was done following the derivation from Borcia et al.[4] Therefore, the solid surface wettability can be set to model contact angle of 0° at $\rho_b = \rho_L$ and 180° at $\rho_b = \rho_V$.

To make equations dimensionless we scale length, time, and density field, and velocity field by characteristic values of unit length (h_0), unit time ($\frac{\rho_c h_0^2}{\eta_L}$), critical density (ρ_c), and ($\frac{\eta_L}{\rho_c h_0}$) correspondingly. A hat above symbols indicates scaled quantities:

$$r = h_0\hat{r};\ \nabla = h_0^{-1}\nabla;\ \rho = \rho_c\hat{\rho};\ t = \frac{\rho_c h_0^2}{\eta_L}\hat{t};\ u = \frac{\eta_L}{\rho_c h_0}\hat{u}$$

Table S1 includes the parameter values used in simulations.

Table S1. Parameters used in simulations

Parameter	Value	Parameter	Value
M_w	$0.018\ kg \cdot mol^{-1}$	$C_1(T = 50°C)$	0.3968
a	$0.28\ J \cdot m^3 \cdot mol^{-2}$	$C_2(T = 50°C)$	0.2124
b	$1.87 \times 10^{-5}\ m^3 \cdot mol$	$C_3(T = 50°C)$	2.1911
$\eta_L(T = 50°C)$	$0.000577\ Pa \cdot s$	$C_4(T = 50°C)$	1.5804
$\eta_V(T = 50°C)$	$0.00001052\ Pa \cdot s$	$C_1(T = 150°C)$	0.4434
$\eta_L(T = 150°C)$	$0.0001867\ Pa \cdot s$	$C_2(T = 150°C)$	0.3343
$\eta_V(T = 150°C)$	$0.00001388\ Pa \cdot s$	$C_3(T = 150°C)$	1.9633
ρ_c	$322\ kg \cdot m^3$	$C_4(T = 150°C)$	1.4778
h_0	$10^{-8}\ m$	$\delta(T = 50°C)$	$2.74 \times 10^{-9}\ m$
$\gamma(T = 50°C)$	$0.0679\ N \cdot m^{-1}$	$\delta(T = 150°C)$	$2.94 \times 10^{-9}\ m$
$\gamma(T = 150°C)$	$0.0482\ N \cdot m^{-1}$		

Numerical implementation. To implement the model the finite volume approach was used within the software package FiPy.[5] The single component liquid-vapor system follows van der Waals thermodynamic theory (equation S2). The governing equations were implemented following the work of Wheeler et al.[3] Each process in simulations was run for 1000 s that roughly corresponds to the observations in experiment. The mesh size used in simulation corresponds to the 1440x480 grid with unit length $h_0 = 10\ nm$. All boundaries set to zero flux boundary condition for dimensionless density $\hat{\rho}$ order parameter.

2. Experimental details

Samples. MgO crystals used in our experiments were grown using the carbon-arc fusion technique at Oak Ridge National Laboratory.[6] The crystals were synthesized in 1996. Therefore, at the time when experiments were conducted the MgO crystals were exposed to air at ambient conditions for 27 years.

Prior to experiments, MgO crystals were cleaved to size of approximately 3 mm blocks and cleaned by sonication in isopropanol for 5 minutes.

Experimental setup. Prepared single crystals were placed in glass vials as showed in the schematic (**Fig.1a**). These vials are kept in a stainless-steel pressure vessel. The pressure vessel filled with deionized water such that vials are in partially submerged state. After airtight sealing of the pressure vessel, they kept in a furnace to heat at 50 ^{o}C and 150 ^{o}C over 48 and 96 hours (**Fig.S1**). To minimize temperature gradient in the pressure vessel, sealed pressure vessel was preheated to target temperature before placing them in the furnace. When heated, water vapor generated in the vessel interacts with the MgO crystal in the vials. Depending on the heating temperature, amount of the saturated vapor density will MgO crystal will vary thus effect the MgO transformation.

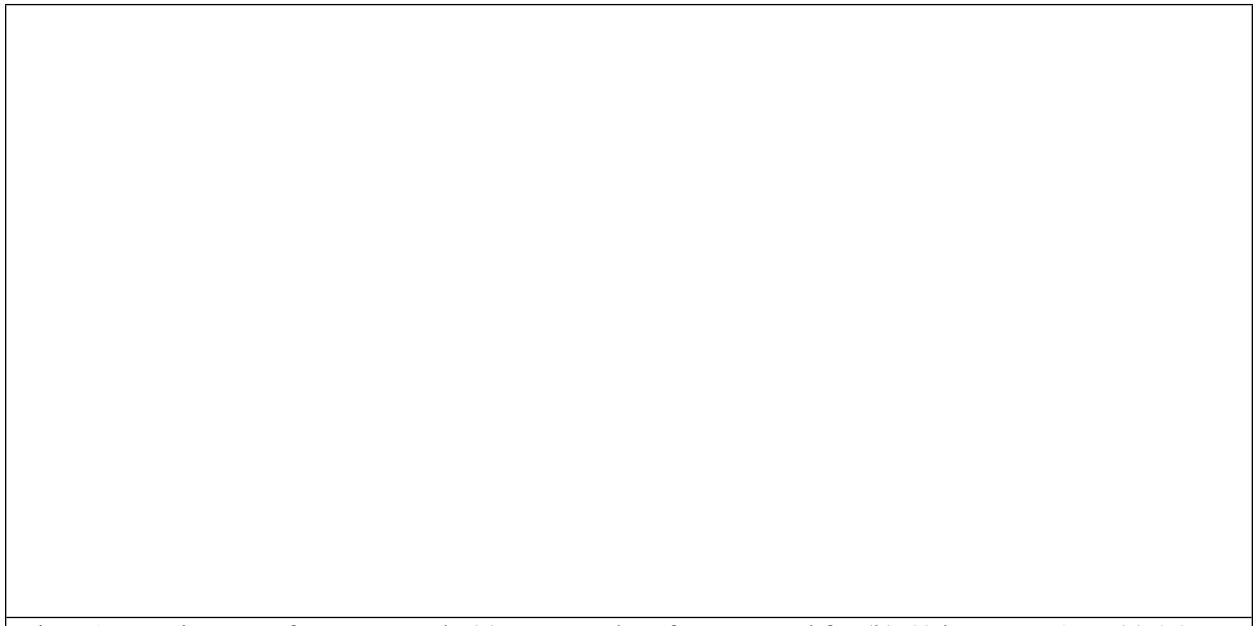

Fig. S1 SEM images of MgO crystals (a) unreacted surface; reacted for (b) 48 hours at 50^{o}C, (c) 96 hours at 50^{o}C, (d) 48 hours at 150^{o}C, and (e) 96 hours at 150^{o}C.

The vapor density is smaller at lower temperatures (50^{o}C, ~0.1 bar) than at higher temperatures (150^{o}C, ~5 bar) casing adsorbed water molecules to form localized droplets instead of thin films. These localized droplets reacted with the MgO surface, transforming it to $Mg(OH)_2$ (**Fig.S1b,c**). At higher temperatures water molecules form a thin film and transform the MgO surface uniformly (**Fig.S1d,e**).

Contact Angle Measurements. A KRÜSS DSA 30 contact angle goniometer equipped with a CCD camera and automated liquid handling controls was used to measure contact angles. Contact angles were measured on 1) freshly cleaved MgO single crystals and 2) MgO single crystals aged for 27 years (previously characterized in Weber et al, 2023)[7]. This MgO crystal exhibits a ~1.5 μm thick reaction layer consisting of hydrated Mg-carbonates.

Fig. S2 Contact angle measurements on MgO exposed to air for 27 years.

Contact angle measurements on MgO exposed to air at ambient conditions for 27 years are shown in **figure S2**. The range of measured angle values vary between 62° (**Fig.S2a**), 75° (**Fig.S2b,c**), and 91° (**Fig.S2d**).

Contact angle measurements on freshly cleaved MgO crystal are shown in **figure S3**. Contact angles measures on freshly cleaved surface consistently demonstrate larger values. The range of measured angle values vary between 83° (**Fig.S3b**) and 97° (**Fig.S3a**).

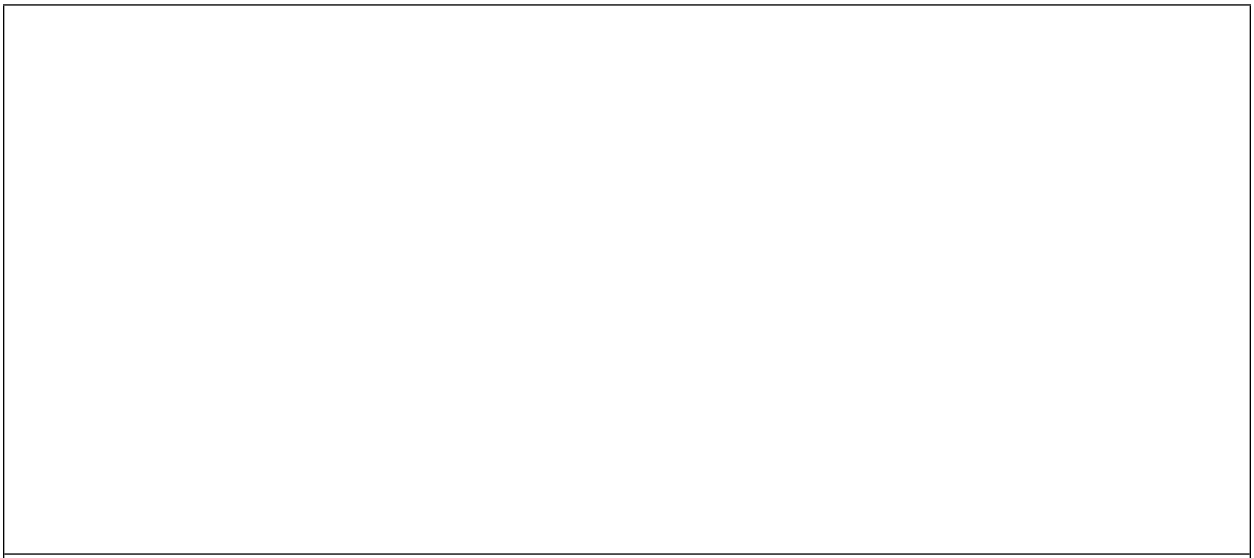

Fig. S3 Contact angle measurements on freshly cleaved MgO.

Characterization of reaction products using Raman spectroscopy. To identify the newly formed surface layer phase, Raman spectroscopy was conducted using a Renishaw InVia Raman instrument equipped with a 532 nm laser, 2400 lines/mm grating and edge filter. Peak positions were calibrated using a Si standard prior to data collection. Data was collected and background subtracted using Renishaw integrated WiRE software. Peak positions were fit using IGOR software and compared with literature.[8]

Fig. S4 Raman characterization of MgO reacted in vapor for 150°C for 2 days. Two different locations on the sample were measured. a) and c) show light microscopy images of the measurement position, which is in the center of the image. b and d show Raman spectra with peak positions typical for brucite at 278 and 443 cm^{-1} matching literature data.[8]

References

1. J. D. van der Waals and J. D. van der Waals, *Journal of Statistical Physics 1979 20:2*, 1979/02, **20**.
2. A. G. Lamorgese and R. Mauri, *Physics of Fluids*, 2009, **21**, 044107-044107.
3. D. Wheeler, J. A. Warren and W. J. Boettinger, *Physical Review E*, 2010, **82**, 051601.
4. R. Borcia, I. D. Borcia and M. Bestehorn, *Phys Rev E Stat Nonlin Soft Matter Phys*, 2008, **78**, 066307.
5. J. E. Guyer, D. Wheeler and J. A. Warren, *Computing in Science and Engineering*, 2009, **11**, 6-15.
6. M. M. Abraham, C. T. Butler and Y. Chen, *The Journal of Chemical Physics*, 1971, **55**, 3752-3756.
7. J. Weber, V. Starchenko, K. Yuan, L. M. Anovitz, A. V. Ievlev, R. R. Unocic, A. Y. Borisevich, M. G. Boebinger and A. G. Stack, *Environ Sci Technol*, 2023, **57**, 14929-14937.
8. C. J. Liu, D. J. Wang, H. F. Zheng and T. Liu, *Phys Chem Miner*, 2017, **44**, 297-306.